# RESEARCH ARTICLE

# **Epilepsia**<sup>™</sup>

# Flexible, high-resolution cortical arrays with large coverage capture microscale high-frequency oscillations in patients with epilepsy

```
Katrina J. Barth<sup>1</sup> | James Sun<sup>2</sup> | Chia-Han Chiang<sup>1</sup> | Shaoyu Qiao<sup>2</sup> | Charles Wang<sup>1</sup> | Shervin Rahimpour<sup>3,4</sup> | Michael Trumpis<sup>1</sup> | Suseendrakumar Duraivel<sup>1</sup> | Agrita Dubey<sup>5</sup> | Katie E. Wingel<sup>5</sup> | Alex E. Voinas<sup>2</sup> | Breonna Ferrentino<sup>2</sup> | Werner Doyle<sup>6</sup> | Derek G. Southwell<sup>7,8</sup> | Michael M. Haglund<sup>8</sup> | Matthew Vestal<sup>8,9</sup> | Stephen C. Harward<sup>8</sup> | Florian Solzbacher<sup>4,10,11</sup> | Sasha Devore<sup>12</sup> | Orrin Devinsky<sup>6,12,13</sup> | Daniel Friedman<sup>12</sup> | Bijan Pesaran<sup>5</sup> | Saurabh R. Sinha<sup>14</sup> | Gregory B. Cogan<sup>8,15,16,17,18</sup> | Justin Blanco<sup>19</sup> | Jonathan Viventi<sup>1,7,8,15,16</sup> |
```

# Correspondence

Justin Blanco, Department of Electrical and Computer Engineering, United States Naval Academy, 105 Maryland Avenue, Annapolis, MD 21402, USA. Email: blanco@usna.edu

Jonathan Viventi, Department of Biomedical Engineering, Duke

# **Abstract**

**Objective:** Effective surgical treatment of drug-resistant epilepsy depends on accurate localization of the epileptogenic zone (EZ). High-frequency oscillations (HFOs) are potential biomarkers of the EZ. Previous research has shown that HFOs often occur within submillimeter areas of brain tissue and that the coarse spatial sampling of clinical intracranial electrode arrays may limit the accurate

© 2023 International League Against Epilepsy.

wileyonlinelibrary.com/journal/epi Epilepsia. 2023;64:1910–1924.

<sup>&</sup>lt;sup>1</sup>Department of Biomedical Engineering, Duke University, North Carolina, Durham, USA

<sup>&</sup>lt;sup>2</sup>Center for Neural Science, New York University, New York, New York, USA

<sup>&</sup>lt;sup>3</sup>Department of Neurosurgery, Clinical Neuroscience Center, University of Utah, Utah, Salt Lake City, USA

<sup>&</sup>lt;sup>4</sup>Department of Biomedical Engineering, University of Utah, Utah, Salt Lake City, USA

<sup>&</sup>lt;sup>5</sup>Department of Neurosurgery, Perelman School of Medicine, University of Pennsylvania, Pennsylvania, Philadelphia, USA

<sup>&</sup>lt;sup>6</sup>Department of Neurosurgery, NYU Langone Health, New York, New York, USA

<sup>&</sup>lt;sup>7</sup>Department of Neurobiology, Duke University School of Medicine, North Carolina, Durham, USA

<sup>&</sup>lt;sup>8</sup>Department of Neurosurgery, Duke University School of Medicine, North Carolina, Durham, USA

<sup>&</sup>lt;sup>9</sup>Department of Pediatrics, Duke University School of Medicine, North Carolina, Durham, USA

<sup>&</sup>lt;sup>10</sup>Department of Electrical and Computer Engineering, University of Utah, Utah, Salt Lake City, USA

<sup>&</sup>lt;sup>11</sup>Department of Materials Science and Engineering, University of Utah, Utah, Salt Lake City, USA

<sup>&</sup>lt;sup>12</sup>Department of Neurology, NYU Grossman School of Medicine, New York, New York, USA

<sup>&</sup>lt;sup>13</sup>Comprehensive Epilepsy Center, NYU Langone Health, New York, New York, USA

<sup>&</sup>lt;sup>14</sup>Department of Neurology, Perelman School of Medicine, University of Pennsylvania, Pennsylvania, Philadelphia, USA

<sup>&</sup>lt;sup>15</sup>Duke Comprehensive Epilepsy Center, Duke University School of Medicine, North Carolina, Durham, USA

<sup>&</sup>lt;sup>16</sup>Department of Neurology, Duke University School of Medicine, North Carolina, Durham, USA

<sup>&</sup>lt;sup>17</sup>Department of Psychology and Neuroscience, Duke University, North Carolina, Durham, USA

<sup>&</sup>lt;sup>18</sup>Center for Cognitive Neuroscience, Duke University, North Carolina, Durham, USA

<sup>&</sup>lt;sup>19</sup>Department of Electrical and Computer Engineering, United States Naval Academy, Maryland, Annapolis, USA

University, 1149 CIEMAS, 101 Science Dr., Durham, NC 27705, USA. Email: j.viventi@duke.edu

### **Funding information**

American Epilepsy Society; Centers for Disease Control and Prevention, Grant/ Award Number: U48DP006396-01SIP 19-003; Epilepsy Foundation; Finding A Cure for Epilepsy and Seizures; National Institutes of Health, Grant/ Award Number: 1R01-DC019498-01A1, 1UG3NS120172, K12 NS080223, R01 HL151490, R01 MH107396, R01 MH111417, R01 MH116978, R01 NS062092, R01 NS06209207, R01 NS104923, R01 NS109367, RF1 MH116978, T32 GM136573, U01 NS090415, U01 NS099577, U01 NS099697, U01 NS099705, U01 NS103518, U01 NS122123, U01 NS123668, R01 DC019498, UG3 NS120172 and UL 1TR002553; National Science Foundation, Grant/ Award Number: CBET-1752274. DGE-1644868, IIS-2113271 and IOS-1557886; U.S. Department of Defense, Grant/Award Number: EP200077; Vilcek Foundation: Tuberous Sclerosis Alliance; Office of Naval Research; Templeton World Charity Foundation; Army Research Office, Grant/Award Number: 68984-CS-MUR; Esther A. & Joseph Klingenstein Fund; Clinical and Translational Science Awards, Grant/ Award Number: UL1TR002553

capture of HFO activity. In this study, we sought to characterize microscale HFO activity captured on thin, flexible microelectrocorticographic ( $\mu$ ECoG) arrays, which provide high spatial resolution over large cortical surface areas.

**Methods:** We used novel liquid crystal polymer thin-film  $\mu$ ECoG arrays (.76–1.72-mm intercontact spacing) to capture HFOs in eight intraoperative recordings from seven patients with epilepsy. We identified ripple (80–250 Hz) and fast ripple (250–600 Hz) HFOs using a common energy thresholding detection algorithm along with two stages of artifact rejection. We visualized microscale subregions of HFO activity using spatial maps of HFO rate, signal-to-noise ratio, and mean peak frequency. We quantified the spatial extent of HFO events by measuring covariance between detected HFOs and surrounding activity. We also compared HFO detection rates on microcontacts to simulated macrocontacts by spatially averaging data.

**Results:** We found visually delineable subregions of elevated HFO activity within each  $\mu$ ECoG recording. Forty-seven percent of HFOs occurred on single 200- $\mu$ m-diameter recording contacts, with minimal high-frequency activity on surrounding contacts. Other HFO events occurred across multiple contacts simultaneously, with covarying activity most often limited to a .95-mm radius. Through spatial averaging, we estimated that macrocontacts with 2–3-mm diameter would only capture 44% of the HFOs detected in our  $\mu$ ECoG recordings. **Significance:** These results demonstrate that thin-film microcontact surface arrays with both highresolution and large coverage accurately capture microscale HFO activity and may improve the utility of HFOs to localize the EZ for treatment of drug-resistant epilepsy.

# KEYWORDS

drug-resistant epilepsy, high-frequency oscillations, interictal, intraoperative, microelectrocorticography

# 1 | INTRODUCTION

The rate of drug-resistant epilepsy has remained stagnant at 30% for several decades despite the development of novel drugs.<sup>1-3</sup> Improving outcomes from surgical treatments, such as resection surgery, laser ablation, and responsive neurostimulation, therefore remains critical to the treatment of drug-resistant epilepsy. 3-7 However, outcomes from surgical approaches are imperfect, with 30%–70% of patients seizure-free after surgical resection, 64% of patients achieving Engel I outcome from laser ablation, and 18% of patients seizure-free for at least 1 year when implanted with a responsive neurostimulator. 7-9 The efficacy of these treatments depends on accurate localization of the epileptogenic zone (EZ), which is the theoretical total area of brain necessary and sufficient for seizure generation. 3,5,6,10,11 The EZ may be approximated by the seizure onset zone (SOZ) but is often

# **Key Points**

- In intraoperative  $\mu ECoG$  array recordings, HFOs most often occurred within a <1-mm radius.
- We observed microscale spatial heterogeneity of HFO activity that would likely be missed by conventional macrocontacts.
- µECoG arrays with high spatial resolution and large coverage could offer a valuable tool for capturing microscale HFO activity to aid mapping of epileptic cortex.

distributed into multiple discrete subregions. <sup>10</sup> A better understanding of interictal activity may aid in the localization of multiple foci of the EZ. <sup>12</sup> High-frequency



oscillations (HFOs) are paroxysmal oscillations in the 80-600-Hz band, which stand out from background activity and may be a biomarker of the EZ. 13-17 Various studies show that interictal HFOs occur at higher rates and amplitudes within SOZ tissue and that resections removing areas with high rates of HFOs, recorded intraoperatively or from implanted arrays during presurgical monitoring, result in improved surgical outcomes. 13-23 HFOs are often subcategorized by frequency as ripples (80-250 Hz) and fast ripples (250-600 Hz), and some studies have shown that fast ripples may be a particularly strong biomarker of the EZ and useful for intraoperative tailoring of the resection margins.<sup>21,23</sup>

However, the use of HFOs as an interictal biomarker has not been widely adopted as a part of clinical presurgical or intraoperative evaluation. This is in part because many studies have relied on group statistics across patients, making it difficult to use HFOs for delineation of the EZ on an individual patient level.<sup>24,25</sup> In particular, recent results of an HFO clinical trial showed that HFOs captured intraoperatively on macrocontact arrays do not perform as well as interictal discharges for tailoring epilepsy surgery. 25 To record HFOs, these studies have primarily used stereoelectroencephalographic (sEEG) arrays with cylindrical contacts of height 1.3-2.4 mm and circumference 3.5 mm spaced 5-10 mm apart or standard clinical electrocorticographic (ECoG) arrays with 2.3-mm diameter contacts spaced 10 mm apart, although ECoG arrays with spacing as low as 3 mm have been used clinically. 17,26-29 We hypothesize that macroelectroencephalographic recordings may capture HFO activity with inadequate spatial precision and therefore have limited the utility of HFOs for clinical delineation of the EZ at an individual patient level.

This hypothesis is supported by previous work demonstrating the microscale nature of HFOs. 30-33 Schevon et al.31 recorded from very small penetrating microelectrode arrays (.4-mm spacing, 16-mm<sup>2</sup> coverage) implanted in the cortex of patients with epilepsy and found that the majority of HFOs (88%) occurred on only 1-2 channels at a time. Yang et al.<sup>33</sup> used very dense, small coverage surface microelectrocorticographic (µECoG) arrays (.05-mm spacing, ~.25-mm<sup>2</sup> coverage) to record interictal activity intraoperatively and found that HFOs occurred in small, repeated spatiotemporal patterns that on average involved <14 channels (~.09 mm<sup>2</sup> tissue). Worrell et al.<sup>32</sup> found that 83% of HFOs occurred on a single microwire (1-mm spacing) at a time, and that 74% of HFOs were captured on microwires compared with 26% on macrocontacts. Although this prior work has been highly valuable in characterizing the microscale occurrence of HFOs, the arrays used in each of these studies lack the broad spatial coverage needed to fully characterize HFO activity at a clinically usable scale

across distributed areas of epileptic cortex. Here, we show the capability of a novel, thin-film surface µECoG array to capture microscale HFO activity both with high resolution and across larger cortical areas.

We captured HFOs during brief intraoperative recordings from patients undergoing resection surgery for epilepsy using liquid crystal polymer thin-film (LCP-TF) μECoG arrays with high resolution (.76–1.72-mm pitch) and large spatial coverage (144-1596 mm<sup>2</sup>) designed for use in the intraoperative setting. 34,35 We identified ripple and fast ripple HFO events using a common automated detection algorithm along with artifact rejection methods. 36-39 We found microscale heterogeneity in HFO characteristics across the arrays, with distinct subregions of elevated activity. HFOs predominantly occurred at the submillimeter scale, with 47% of events occurring on only one 200-µm-diameter contact at a time without activity detected on neighboring contacts .76-1.72 mm away. HFOs with activity beyond one contact typically occurred within a .95-mm radius, an area smaller than the space between clinical macrocontacts. We have also demonstrated through spatial averaging that standard clinical macrocontact arrays would likely miss many of the microscale HFOs captured on our μECoG arrays. Our results support the use of high-resolution, broad coverage recording arrays to capture interictal activity in finer detail during electroencephalographic evaluation of patients with epilepsy. Future research using high-resolution arrays, both intraoperatively and during presurgical monitoring, may further elucidate the relationship between HFOs and the SOZ to improve diagnostic targeting for the treatment of drug-resistant epilepsy.

# MATERIALS AND METHODS

### 2.1 **Subjects**

We evaluated HFO activity in intraoperative µECoG recordings from seven patients (Table 1; three females; median age=41 years, range=14-49 years) undergoing surgical intervention for drug-resistant epilepsy at Duke University Medical Center or NYU Langone Health. One subject (S1) had two separate recordings collected from two different locations within the craniotomy, differentiated as S1A and S1B (Table 1). Informed consent was obtained in a manner approved by each institution's institutional review board.

### LCP-TF µECoG arrays 2.2

We used LCP-TF µECoG arrays described previously to record intraoperatively from the surface of the brain in each



		,							
Subject	Age, years	Sex	Recording time, min	Array location	SOZ location	Clean channels/ total channels, n	Pitch, mm	Anesthesia state	Surgical drugs
S1A	41	ഥ	5.48	L supramarginal gyrus	L inferior precentral gyrus	218/244	.76	Anesthetized	Sevoflurane (1.64%) Remifentanil (.05 μg/kg/min) Dexmedetomidine (.2 μg/kg/h)
S1B	41	ഥ	5.11	L inferior precentral gyrus	L inferior precentral gyrus	218/244	.76	Anesthetized	Sevoflurane (1.64%) Remifentanil (.05 μg/kg/min) Dexmedetomidine (.2 μg/kg/h)
S2	49	Ц	10.67	L anterior inferior temporal gyrus	L inferior temporal gyrus	221/244	.76	Anesthetized	Propofol (130 µg/kg/min) Remifentanil (.125 µg/kg/min)
S3	34	M	18.08	L posterior superior temporal gyrus	L mesial temporal lobe	223/244	.76	Awake	Remifentanil (.02 µg/kg/min)
S4	41	Щ	18.43	L posterior superior temporal gyrus	L mesial temporal lobe	241/256	1.72	Anesthetized	Isoflurane (.08%)
S5	19	$\mathbb{Z}$	12.00	L posterior inferior parietal lobe	L superior parietal lobe; superior posterior occipital lobe	229/244	.76	Anesthetized	Propofol (80 µg/kg/min) Remifentanil (.3 µg/kg/min) Dexmedetomidine (1.5 µg/kg/h)
Se	14	M	16.27	R anterior superior temporal gyrus	R middle temporal gyrus	251/244	1.72	Anesthetized	Sevoflurane (2.4%) Rocuronium (10 µg)
S7	47	M	14.13	L lateral temporal lobe	L lateral temporal lobe (lesional)	345/512	1.72	Awake	Clevidipine (6 mg/h)
A lab more de 41 ou	formed to	T 100. M	Atheres of the Company of the Manager of the Company of the Compan	70000					

Abbreviations: F, female; L, left; M, male; R, right; SOZ, seizure onset zone.



of use; OA articles are governed by the applicable Creative Commons

subject (Figure 1).34,35,40 Custom arrays were fabricated by DYCONEX (Micro Systems Technologies). We used three μECoG array designs with different center-to-center spacings (pitches) and coverages to fit each craniotomy and recording target. These included a 244-contact design with 12×12-mm coverage and .76-mm pitch (Figure 1A), a 256-contact design with  $21 \times 38$ -mm coverage and 1.72-mm pitch (Figure 1B), and a 512-contact design created by joining two 256-contact arrays together, giving a total coverage of 42×38mm and 1.72-mm pitch (Figure 1B). All arrays had 200-µm-diameter gold or platinum-iridium recording contacts. Arrays were coated in silicone (polydimethylsiloxane MDX4-4210, USP class VI, Dow Corning) per previously reported methods to create unique mechanical configurations, join multiple arrays together, and soften the thin edges of the arrays to prevent any small incisions to tissue. 41 See Appendix S1 and Figure S13 for additional details on in vitro device testing.

# 2.3 | Intraoperative data collection

We connected each  $\mu$ ECoG array to custom recording headstages using either ultra-low-profile compression connectors (ZA8, Samtec) or zero-insertion-force connectors (ZIF FH43B, Hirose). The headstages had digital electrophysiology interface chips (RHD2164, part #D8215, Intan Technologies) for amplification and digitization as described in Chiang et al.<sup>34</sup> The cable length between the electrode array and headstage boards was 40 mm in all electrode designs (Figure 1A,B). Headstages were

housed in custom three-dimensionally (3D) printed casings (Figure 1C; Duraform PA, 3D Systems-Quickparts). Micro High-Definition Multimedia Interface (µHDMI) cables were used to connect the headstage assemblies to the recording controller (1024ch RHD Recording Controller, part #C3008, Intan Technologies), which remained outside the sterile zone for data acquisition (RHD and RHX Data Acquisition Software, Intan Technologies) by the research team (Figure 1D). The LCP-TF arrays, encased headstage assemblies, and µHDMI cables were sterilized prior to surgery using either ethylene oxide or hydrogen peroxide (Figure 1C,E-G). All data were collected at a sampling rate of 20 kilosamples per second (kSPS), with hardware filtering from .1 Hz to 7.5 kHz or 10 kHz. The surgeon used a sterilized alligator clip to connect a shared ground and reference pin on the recording headstages to a metal scalp retractor in contact with the patient's scalp and skull. For each recording, the surgeon placed the µECoG array on the area of exposed cortex nearest the clinically determined SOZ as allowed by the constraints of the craniotomy, except for S1A, in which the array was placed over an area of high interictal activity (Table 1). The SOZ was determined by neurologists at each respective institution from either presurgical intracranial monitoring with clinical stereo or grid arrays or identification of a clear lesion on the preoperative magnetic resonance imaging (MRI). In two subjects (S3 and S7), intraoperative recordings were collected while the patient was awake for clinical mapping (Table 1). All other subjects were anesthetized during the research recording period. All recordings were

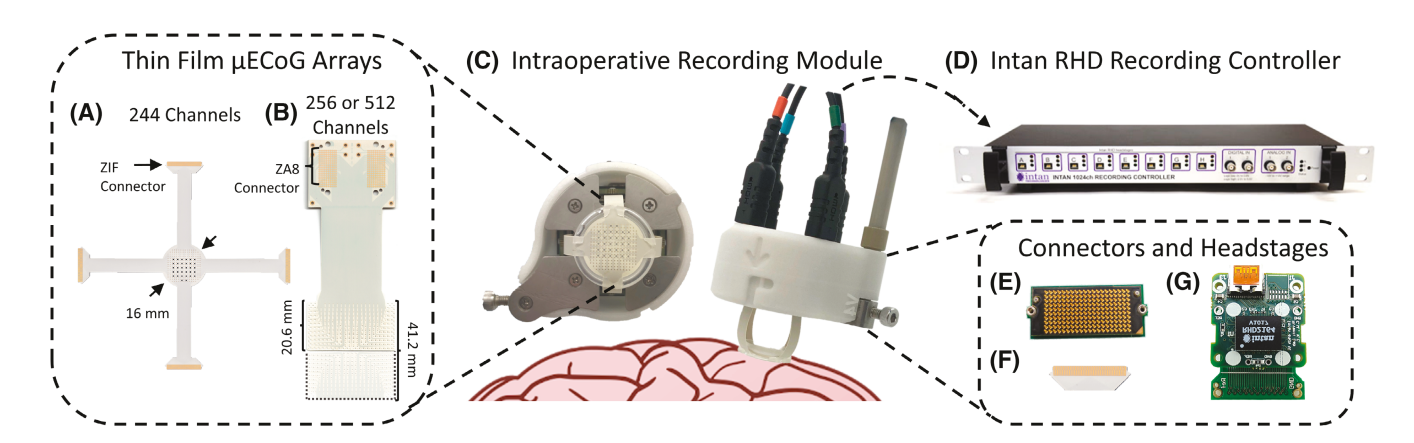


FIGURE 1 Intraoperative recording setup with liquid crystal polymer thin-film (LCP-TF) microelectrocorticographic (μΕCoG) arrays. We used three different LCP-TF μΕCoG array designs for intraoperative recordings: (A) a 244-channel array with .76-mm pitch, (B) a 256-channel array with 1.72-mm pitch, and a 512-channel array shown in semitransparency created by combining two 256-channel arrays for larger coverage. (C) The LCP arrays are molded with polydimethylsiloxane silicone and connected to the recording headstage module. Custom three-dimensionally printed casings enclose the headstages with a ground screw extended from the side. An example is shown of the 244-channel array from (A) molded and attached to headstages. (D) The headstage module connects to the Intan RHD Recording Controller through micro High-Definition Multimedia Interface cables shown in (C) and Serial Peripheral Interface cables. (E) A Samtec ZA8 Ultra Low-Profile Compression Connector is used to connect the 256-channel arrays to the custom headstage board shown in G. (F) A Zero Insertion Force connector used to connect the 244-channel array to the custom headstage board. (G) The custom headstage board, which uses a 64-channel Intan RHD chip for amplification and analog to digital conversion. This figure is adapted from Sun et al. 35



15281167, 2023, 7, Downloaded from https://onlinelibrary.wiley.com/doi/10.1111/epi.17642 by Duke University Libraries, Wiley Online Library on [24/10/2024]. See the Terms and Condit

of use; OA articles are governed by the applicable Creative Commons License

collected intraoperatively without any electrographic seizure activity present and therefore considered interictal.

### Data preprocessing 2.4

Data were analyzed using both previously published and custom MATLAB code (MathWorks).37 Each recording was decimated to 2 kSPS (Chebyshev type I infinite impulse response filter of order 8). Channels were excluded from analvsis if the contact impedance at 1 kHz exceeded 500 kOhm, measured either intraoperatively or postoperatively, or if the channel exhibited visually evident high-frequency noise (Table 1). Time segments with large artifacts across all channels, typically resulting from movement of the array or ground cables, were cut out of the recording.

### 2.5 HFO detection and artifact rejection

We detected candidate HFOs in our µECoG recordings using a previously published and widely cited energy thresholding algorithm developed by Staba et al. 31,32,36,37,42 We implemented this algorithm in the ripple (80-250 Hz) and fast ripple (250-600 Hz) frequency bands using previously published open-source software (RippleLab version 3, accessed July 2020; https://github.com/BSP-Unian des/RIPPLELAB/).<sup>37</sup> We then took two additional steps to eliminate widely reported false positive HFO detections resulting from the ringing artifacts due to filtering sharp transients and spikelike waveforms. 38,39,43,44 First, we eliminated HFO detections for which the derivative of the unfiltered signal surpassed 150 µV/ms (Figure 2D). Second, we visually reviewed and excluded any remaining HFO events resulting from sharp transients and spikelike waveforms with continuous power from the low- to high-frequency bands (Figure 2E). Elimination of spikelike waveforms during visual review could complicate the identification of coincident ripple-on-spike events. We differentiated HFOs coincident with, rather than resulting from the filtering of, spikelike waveforms by the presence of a clear HFO in the raw signal and/or a spectral "island" independent from the broader signature of the spike in the time-frequency plots (Figure 2A-C). 38,43,45 Further

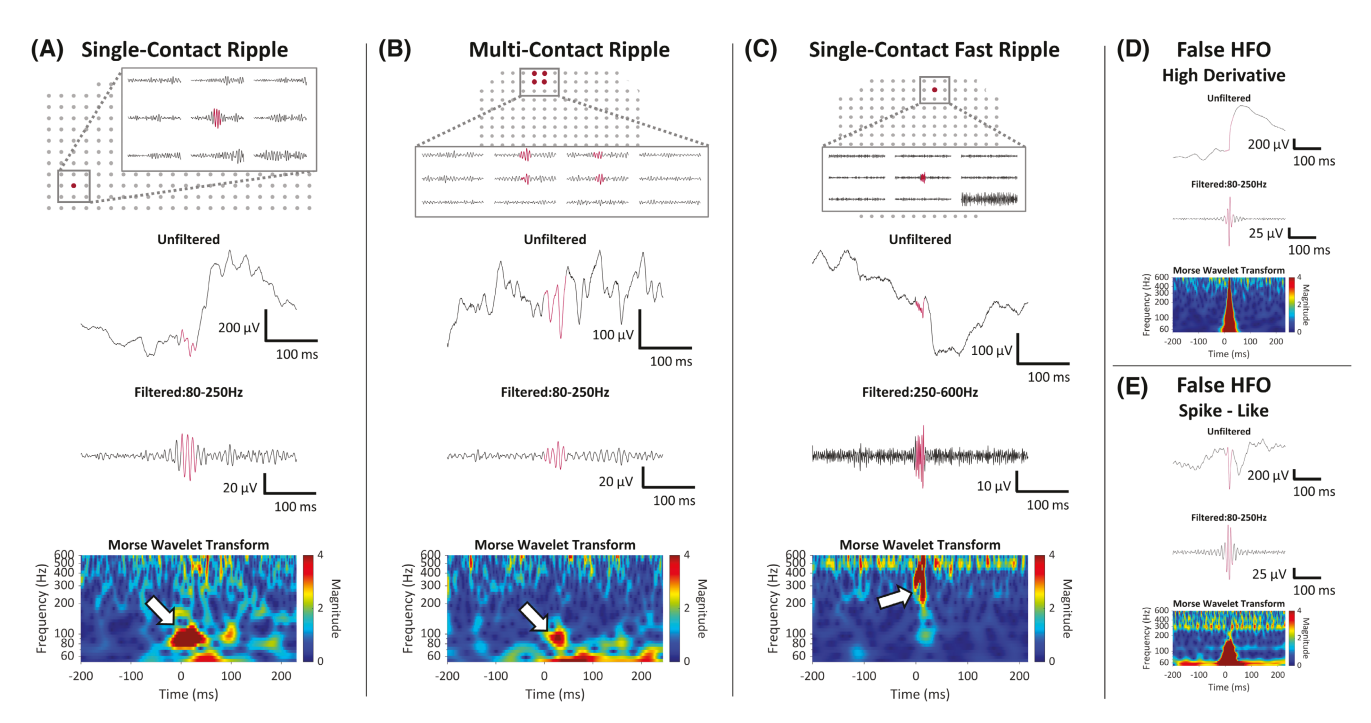


FIGURE 2 True and false high-frequency oscillations (HFOs) detected in microelectrocorticographic recordings. (A) An example from S4 of a ripple HFO occurring on a single 200-µm-diameter microcontact. (B) An example from S5 of a ripple HFO occurring across multiple microcontacts. The upper left HFO is shown in further detail in the plots below. (C) An example from S3 of a fast ripple HFO occurring on a single 200-µm-diameter microcontact. The channel in the bottom right corner of the first inset was excluded from analysis due to high baseline noise in the 80-600-Hz band. (D) An example from S5 of a false HFO detection due to a sharp transient, which was removed by derivative thresholding. (E) An example from S6 of a false HFO detection due to a spikelike waveform, which was removed by visual review. Shown in panels A and C from top to bottom: array position of the HFO and surrounding activity, the unfiltered signal corresponding to the HFO detection in red, the filtered (80-250 or 250-600 Hz) HFO signal in red, and the time-frequency plot of the HFO with a spectral island indicated with a white arrow. The time axis is aligned across the bottom three plots, with 0 indicating the start of the HFO detection. Shown in panels D and E from top to bottom: the unfiltered signal corresponding to the false ripple HFO detection in red, the filtered (80-250 Hz) false HFO signal in red, and the time-frequency plot of the above signal.





details on our HFO detection method can be found in Appendix S1.

# 2.6 | HFO feature analysis

HFO rate was calculated for each clean contact as the number of HFO events detected per minute of clean recording. HFO root mean squared (RMS) amplitude ( $\mu$ V rms) was calculated in the ripple (80–250 Hz) and fast ripple (250–600 Hz) frequency bands, and power ( $\mu$ V rms²) was calculated as RMS amplitude squared. HFO signal-to-noise ratio (SNR) in decibels was calculated using the following equation:

$$SNR = 20 \times log_{10} \left( \frac{HFO_{rms}}{Baseline_{rms}} \right)$$

HFO<sub>rms</sub> is the RMS amplitude of the HFO event in the respective ripple or fast ripple bandpass filtered signal. Baseline<sub>rms</sub> is the average of RMS amplitude values computed across six 10-s-long baseline recording periods in the bandpass filtered signal. The 10-s baseline segments were randomly selected for each contact and were at least 20 ms apart in time from any HFO event on a given contact. The derivative thresholding criteria was also applied to the baseline segments to eliminate segments with high power in the bandpass filtered signal due to sharp transients. Mean peak frequency was defined as the frequency at which the Morse wavelet transform power was the largest during the HFO duration.

# 2.7 | Cross-covariance analysis

The detection of HFOs by energy thresholding results in binary classification of the signal on each contact as an HFO or not. Lower amplitude high-frequency activity surrounding a high-amplitude detected HFO could have fallen below the amplitude threshold for automated detection but likely reflects the same neural activity as the detected event. We used zero-lag cross-covariance between HFOs and the bandpass filtered signal (80-250 Hz for ripples, 250-600 Hz for fast ripples) on surrounding channels as a method to quantify the continuous, rather than binary, spatial extent of HFO events. If the mean crosscovariance with the bandpass filtered signal on the four contacts most closely neighboring the central HFO (above, below, left, and right) was <20% of the autocovariance of the central HFO, then we labeled the HFO as "single contact." We deemed all other cases multicontact events and fit the following exponential model to the covariance over distance plot to quantify the radial extent of HFO activity for each group:

Covariance = 
$$(a \times e^{-b \times Distance}) + c$$

The a, b, and c variables are coefficients of the exponential fit. The c term was used to allow the exponential model to approach a nonzero value because all contacts had a common mode signal and therefore a nonzero covariance. We used the 1/b value from the exponential model fit, or the distance at which the covariance has decayed to  $\sim 37\%$  of the y-intercept, as a measure of the radial extent of each multicontact HFO event. To characterize the spatial scale of all the multicontact HFO events, a gamma distribution was then fit to a histogram of the length constants and a peak in the distribution was identified (Figure 4C). Further details on the covariance analysis can be found in Appendix S1.

# 2.8 | Spatial averaging analysis

A metal contact placed on or within the brain records the spatial average of the voltage across the contact's area from the local field potential (LFP), which reflects a summation of postsynaptic currents. 46-48 From these principles, we have approximated the LFP signal that would be captured by a macrocontact by spatially averaging the signal across multiple microcontacts that spatially subsample an area equivalent to the size of a hypothetical macrocontact.<sup>29</sup> We simulated recordings with increasingly larger contact size by averaging the unfiltered data from microcontacts in a series of spatial patterns (Figure 5). The schematics in Figure 5A show the grid of contacts included in each spatial averaging pattern. For each pattern, the central contact was replaced by the average of all contacts marked in green (Figure 5). This provided a set of simulated recordings for each subject with the same total number of contacts but each with increasingly larger contact size. Any high-impedance or noisy contacts were filled in with the average of its eight nearest neighbors before spatially averaging the data. The same HFO detection and artifact rejection process was then applied to each set of spatially averaged recordings. For each originally detected HFO event, we determined whether that HFO was still detectable in the spatially averaged data. Because the contacts on the outer four edges of the array would not include the same number of neighbors as the central contacts, HFOs detected on the outer edges were excluded from this analysis. The simulated equivalent macrocontact sizes were estimated by the distance between the furthest two microcontacts in each spatial averaging pattern.



15281167, 2023, 7, Downloaded from https://onlinelibrary.wiley.com/doi/10.1111/epi.17642 by Duke University Libraries, Wiley Online Library on [24/10/2024]. See the Terms

of use; OA articles are governed by the applicable Creative Commons!

### 3 RESULTS

We have evaluated HFOs from eight brief intraoperative recordings of drug-resistant epilepsy patients (seven subjects) using three different µECoG array designs (Table 1, Figure 1). After preprocessing, there was an average clean recording time of 12.2 min (range = 5.1-18.2 min) per subject. After eliminating false oscillations resulting from high-derivative transients and spike-like waveforms, we retained 32% (8272/26245) of the total candidate HFO events flagged by the automated detector for analysis (Figure 2D,E). We found few HFOs coincident with spikes, which we differentiated from false detections by requiring the presence of a distinct spectral

island in the HFO frequency band or an HFO visible in the unfiltered signal. 38,39 Other microcontact HFO studies using the Staba energy thresholding method also reported high rates (~80%) of false positive detections. 32,42 We found that HFOs occurred at various spatial scales, sometimes on only a single microcontact (47%, Figure 2A,C) and other times across multiple microcontacts at once (Figure 2B). HFOs occurred at an average rate of approximately one HFO every two minutes on each microcontact (.50 HFOs/min/contact). However, the rate of HFOs varied greatly both between subjects and across the array within each subject (Figure 3A,D, Figures S1-S8). Overall, we detected 3.2× more ripples than fast ripples (6336/1936 ripples/fast ripples), with the exception

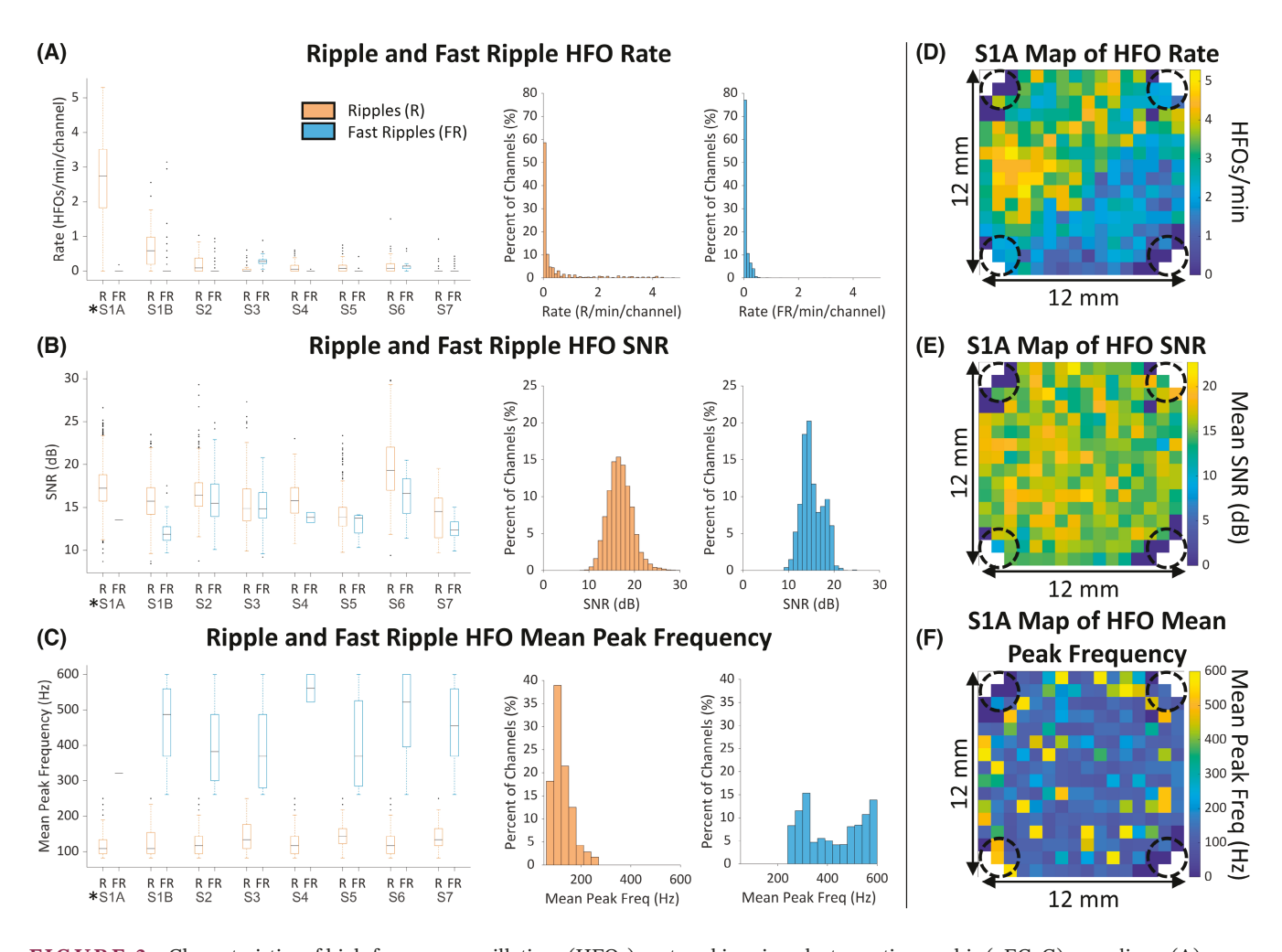


FIGURE 3 Characteristics of high-frequency oscillations (HFOs) captured in microelectrocorticographic (µECoG) recordings. (A) Rate of ripple (R) and fast ripple (FR) HFOs per minute on each channel, shown by subject (left) and across all subjects (right). The asterisk indicates the subject for which further detail is shown in panels D-F. (B) Signal-to-noise ratio (SNR) of R and FR HFOs on each channel over baseline in the respective filter bands (80-250 or 250-600 Hz), shown by subject (left) and across all subjects (right). (C) Mean peak frequency of R and FR HFOs on each channel, determined as the frequency, with maximum coefficient value in the Morse wavelet transform, shown by subject (left) and across all subjects (right). (D) Distinct hotspots of activity can be seen, showing a heatmap of HFO rate (Rs and FRs) on each channel across the array for subject S1A. (E) Heatmap of HFO SNR (Rs and FRs) on each channel across the array for Subject S1A. (F) Heatmap of HFO peak frequency (Rs and FRs) across the array map for Subject S1A. Black dashed circles on each heatmap indicate the relative diameter (2.3 mm) and spacing (10 mm) of a standard clinical ECoG grid for comparison. The µECoG array does not have recording channels in the corner positions shown in white.



Length Constant [mm]

FIGURE 4 Size of high-frequency oscillation (HFO) events measured by cross-covariance. (A) An example of one single-channel HFO event from S5. (B) An example of a multichannel HFO event from S5. This is the same multichannel event shown in Figure 2B. Each heatmap shows cross-covariance values computed between the bandpass filtered signal (80-250 Hz for ripples, 250-600 Hz for fast ripples) on each channel and the central HFO channel indicated in white. Each scatter plot shows the average cross-covariance values across channels that are equidistant from the central HFO channel. Error bars show ±1 SD. For the multichannel example in B, an exponential model fit is shown in gray ( $R^2 = .77$ ). The dashed line indicates the length constant, defined as 1/b coefficient from the exponential fit. (C) The distribution of HFO event size from all events across all subjects. The percentage of HFO events occurring on single channels (left, purple) is shown separately from the multichannel HFO events (right, blue). A gamma fit (solid gray line) is applied to the distribution of length constant values for the multichannel HFO events. The peak of the gamma distribution is indicated by the black dashed line at .95 mm.

Channel

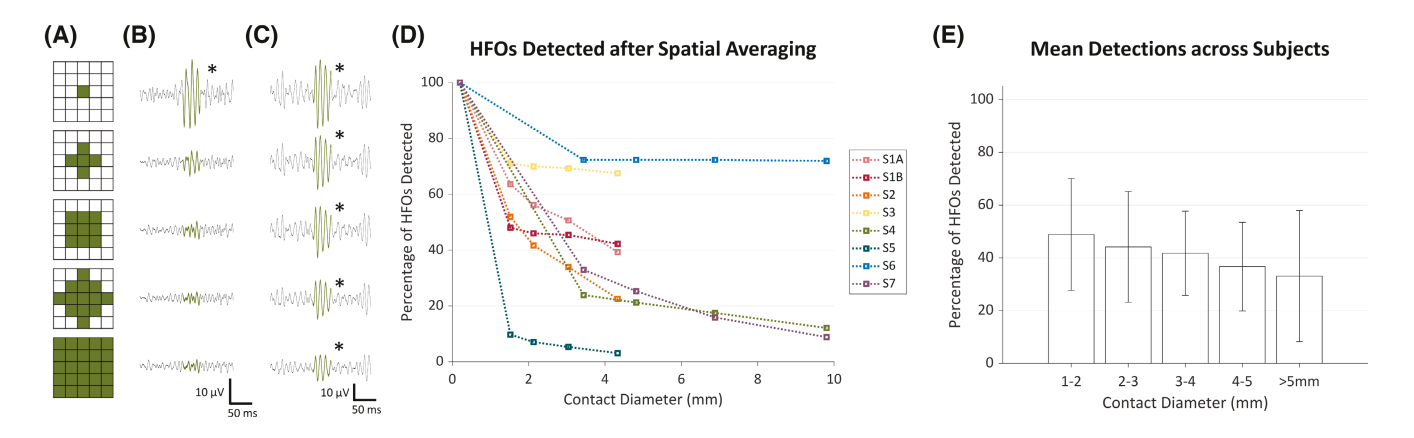


FIGURE 5 Spatial averaging shows that fewer high-frequency oscillations (HFOs) would be detected on macroelectrocorticographic arrays. (A) Schematic of the four spatial averaging patterns. For each stage, the signal on the center channel is replaced by the average of the signal on all channels in green. These grids are not to scale with the actual coverage of the microcontacts averaged in each pattern, but schematically show each spatial averaging filter pattern. (B) An example from S5 of the bandpass filtered (80-250 Hz) signal at each stage of spatial averaging where the ripple HFO was diminished and no longer detected due to spatial averaging. (C) An example from S4 of the bandpass filtered (80-250 Hz) signal at each stage of spatial averaging where the HFO was still detected after spatial averaging. Asterisks indicate detected HFOs. (D) Percentage of the original HFOs detected at each spatial averaging stage for each subject. An estimated equivalent contact diameter was determined from the spatial averaging patterns based on each recording array's pitch. (E) Percentage of the original HFOs across all subjects detected after spatial averaging and binned by estimated equivalent contact diameters. The error bars show  $\pm$  twice the standard error of the mean. The bar representing 1-2-mm contact diameter only reflects data recorded using .76-mm pitch arrays (five of eight recordings), because the first averaging pattern at 1.72-mm pitch exceeds this estimated equivalent diameter. Each contact diameter range includes the lower bound and excludes the upper bound.



of S3, which had a higher rate of fast ripples (Figure 3A). Factors particularly relevant to HFO rate that varied between subjects include brain region recorded and surgical drugs (Table 1). Ripples had an average rate of .44 HFOs/ min/contact (SD = .92 HFOs/min/contact), average amplitude of  $14.5 \,\mu\text{V}$  rms (SD= $7.6 \,\mu\text{V}$  rms), average SNR of 16.9 dB (SD = 2.7 dB), and average mean peak frequency of 124.6 Hz (SD = 38.4 Hz). Fast ripples had an average rate of .062 HFOs/min/contact (SD=.16 HFOs/min/ contact), average amplitude of  $9.3 \,\mu\text{V}$  rms (SD= $3.0 \,\mu\text{V}$ rms), average SNR of 15.2dB (SD=2.4dB), and average mean peak frequency of 422.3 Hz (SD=120.3 Hz; Figure 3, Figure S9). Across subjects, we found that a greater proportion of fast ripples occurred on single microcontacts (mean = 89%, SD = 15%) than did ripples (mean = 35%, SD = 29%, p = .0011 by Wilcoxon rank sum test; Figure S10A). However, we did not find a strong relationship between multichannel HFO event size and peak frequency or HFO power (Figure S10B,C). Representative examples from Subject S1A of the average HFO rate across the 244-contact array show distinct subregions of elevated HFO rate that are smaller than the pitch of clinical macrocontacts (Figure 3D).

As similarly reported in other studies, we observed that some of the contacts surrounding detected HFOs showed oscillatory activity in the 80-250-Hz or 250-600-Hz frequency bands but at a subthreshold level and were therefore unflagged by the automated detection process.<sup>31</sup> To account for this gradual diminishing of the HFO signal across the array, we used cross-covariance to measure the spatial extent of HFOs. The covariance curves in Figure 4 show covariance values averaged between contacts at each distance from the central HFO event. Figure 4A shows an example of an HFO for which the neighboring contacts had covariance values of <20% of the autocovariance and was therefore labeled as a single-contact event. Figure 4B shows an example of an HFO for which the neighboring contacts had covariance values of >20% of the autocovariance and was therefore labeled as multicontact. From this method, we found that 47% of HFOs occurred on single contacts without covarying oscillatory activity on surrounding contacts (Figure 4C). Forty-eight percent of HFO events were multicontact and had radial spatial extents quantified by a length constant value from the exponential fit. A gamma distribution was fit to a histogram of the multicontact length constants (range  $= .4-20 \,\mathrm{mm}$ ), and the peak of the distribution fell at .95 mm (Figure 4C). Sixty-three percent of all characterized HFO events (including single and multicontact) extended over a  $\leq$ 1.0-mm radius, and 98% of all characterized HFO events extended over a ≤5-mm radius. Five percent of HFO events had covariance-distance curves that poorly fit an exponential model as compared to a linear model and were therefore

excluded from these calculations as well as the histogram of multicontact HFO spatial extent shown in Figure 4C.

In all subjects, fewer of the original HFOs were detected as the extent of spatial averaging increased (Figure 5D,E). Figure 5B shows an example of an HFO that would not be detectable at an estimated equivalent contact diameter of 1.52 mm. Figure 5C shows an example of an HFO that would be detectable on an estimated equivalent contact as large as 9.8 mm in diameter. Although the decrease in detected HFOs with increased spatial averaging varied between subjects, across subjects we found that 56% of the HFOs in our  $\mu ECoG$  recordings would be undetectable on clinical standard macrocontacts 2–3 mm in diameter.

# 4 DISCUSSION

Our analysis of HFOs in intraoperative µECoG recordings has shown that HFOs are predominantly a microscale phenomenon and that the use of HFOs to delineate the EZ may be limited by the insufficient spatial sampling of clinical macrocontact arrays. In contrast to previous work evaluating the microscale spatial activity of HFOs, we have captured HFO activity on arrays with both high resolution and large coverage. We identified HFOs in eight intraoperative recordings from patients undergoing surgical treatment for drug-resistant epilepsy and found that the rate of HFOs varied across each array and that subregions of elevated activity, or hotspots, could be visually identified (Figure 3D, Figures S1-S8). We compared the spatial scale of these hotspots with clinical standard ECoG grid contacts (2.3-mm diameter, 10-mm spacing; Figure 3D). Although the positioning of these macrocontacts relative to the µECoG arrays is only hypothetical, this comparison demonstrates that these hotspots are sufficiently small to potentially go uncaptured by clinical standard ECoG grids due to their coarse spatial sampling. We also found differences in the localization of ripples and fast ripples, although the low average rate of fast ripples (.06 fast ripples/channel/min) compared with ripples (.44 ripples/ channel/min) limits this comparison (Figures S1-S8). In addition, we found that 47% of HFOs in our recordings occurred on single 200-µm-diameter contacts without highfrequency activity on surrounding contacts .76-1.72 mm away (Figure 4). In cases when HFOs occurred across multiple microcontacts, their spatial extent was most often limited to a .95-mm radius, much less than the typical 10-mm spacing between clinical macrocontacts (Figure 4). We also demonstrate that macro-ECoG arrays would likely miss the majority of the HFO events captured in our recordings due to the spatial averaging effect of large contacts (Figure 5). Together, our results show two important features of high-resolution arrays over clinical standard



ECoG. First, our HFO event size analysis (Figure 4) demonstrates that higher resolution ensures improved spatial sampling of HFO activity, which may occur in microscale areas and could be missed between largely spaced (10-mm pitch) ECoG macrocontacts. Second, our spatial averaging analysis (Figure 5) shows that small diameter contacts capture microscale HFO signals, which may be effectively attenuated by larger macrocontacts.

Previous studies on HFOs using microelectrode arrays similarly found that HFOs are primarily microscale events.31-33 These studies used arrays with higher density but smaller coverage ( $\leq 4 \times 4$  mm). This in part has limited the clinical translatability of the results for surgical monitoring, which requires sampling large areas of epileptic cortex. The arrays used in this study enable the high-resolution measurement of larger cortical areas, providing recording coverage equivalent to that of standard clinical grids containing 4-16 macrocontacts (148.8-778.7 mm<sup>2</sup>). Furthermore, the arrays studied here can be used in cases with large craniotomies to record from 1024 contacts (3114.7 mm<sup>2</sup>), as described in a previous publication.<sup>34</sup> Our large-coverage, high-resolution μECoG arrays could span both SOZ and non-SOZ regions to assist clinical intraoperative mapping. However, there were several reasons why we were unable to compare HFOs within and outside the SOZ in the present study, including a lack of precise microelectrode placement data for mapping onto MRI and clinical coordinates as well as limited intraoperative craniotomy exposure. Our data are unable to demonstrate clinically significant differences between HFOs of different spatial scales, but we expect that future work recording within and outside of epileptic cortex using large coverage arrays with multiple contact sizes and spacings could address this question.

Our use of cross-covariance as a method for quantifying the spatial extent of HFOs was intended to address a problem observed in our recordings and described by others when characterizing HFOs on high-resolution arrays. Namely, because the detection of HFOs is based on energy thresholding in the 80-600-Hz band, the binary classification of the signal on each contact as an HFO or not depends on the amplitude of the oscillation relative to background activity. Our covariance analysis accounts for the more continuous manifestation of HFO-like activity beyond contacts with detected HFOs. For example, looking closely at the activity across contacts in the HFO event shown in Figure 2B, there are low-amplitude oscillations on several neighboring contacts that resemble the detected HFOs shown in but fell below threshold for detection. If the size of this multicontact event were measured based only on the binary HFO detections, the estimated radius of HFO activity would be ~.54 mm. In contrast, our covariance analysis for this same event shown in Figure 4B

measured a more generous radius of HFO activity of .93 mm. This further strengthens our result, because even when accounting for subthreshold activity on neighboring contacts we find that a majority of HFOs occurred within a <1-mm radius. It should be noted that as in previous literature, our covariance analysis measures HFO event size at a single window of time and would not measure cortical propagation as is commonly investigated in the case of other epileptic activity such as interictal discharges. 31,49 We found that a large majority of neighbors in multichannel HFOs most strongly covaried at a zero-time lag, indicating simultaneous occurrence of HFOs across multiple channels without spatial propagation (Figure S12). However, a minority of HFO events more strongly covaried at a nonzero time lag, indicating the possibility of HFO propagation, which is supported by previous literature (Figure S12).<sup>50</sup> Further research is needed to understand propagation of HFOs at the microscale.

There are several noteworthy limitations to our study design and results. First, although we recorded from within the bounds of the craniotomy in each patient, there were two cases (S3 and S4) in whom the clinically identified SOZ was not directly accessible during the intraoperative µECoG recording (Table 1). However, this does not minimize the significance of our analyses and results, which have characterized the spatiotemporal scale of HFOs, not their clinical significance or specificity to the SOZ. Future work using micro-sEEG would enable additional microscale recordings of the SOZ in mesial temporal lobe cases.<sup>34</sup> Also, although we were not able to directly compare recordings of HFOs on differently sized contacts, we have approximated macrocontact recordings by a previously validated method of averaging the signal between microcontacts over an equivalent macrocontact area.<sup>29</sup> It should be noted that our signal averaging method does not account for the lower impedance and differences in SNR of macrocontacts. The actual signal captured by macrocontacts may differ from our spatial average approximation due to these factors as well as any inhomogeneity of the LFP unsampled between our microcontacts. Our results are supported by a comparison to intraoperative macro-HFO rates from literature. A study of intraoperative standard macro-ECoG recordings from 54 patients found an average rate of 20.6 HFOs/min/contact.<sup>23</sup> The rate of HFOs per area, rather than the rate of HFOs per contact, is a more accurate way of comparing the HFO rate between micro- and macrocontact recording studies. Because one macrocontact on the 10-mm pitch arrays used in the study serves to record activity from a 1-cm<sup>2</sup> area, this is an equivalent rate of 20.6 HFOs/min/cm<sup>2</sup>. In contrast, the average rate of HFOs captured on our µECoG arrays was 98.9 HFOs/min/cm<sup>2</sup>. The comparison between

high- and low-resolution arrays would best be made by simultaneous recordings at the macro and micro spatial scales using a hybrid ECoG array design. 34 Previous work by Worrell et al.<sup>32</sup> using a hybrid sEEG depth electrode showed that microwire contacts recorded a higher rate of HFOs than neighboring macrocontacts, a difference that was statistically significant in the fast ripple band. This is concordant with our finding that a greater proportion of fast ripples occurred on single microcontacts than of ripples (S10A, p = .0011 by Wilcoxon rank sum test). Our spatial averaging analysis has only examined the effect of contact size, not pitch. As demonstrated in Figure 3, macrocontact arrays may miss HFO activity not only due to spatial averaging of the signal but also because of the unsampled gaps between the contacts, typically a 10mm pitch. Therefore, our results may be a conservative estimate of the information lost by macrocontact arrays. The goals of minimizing contact size, minimizing empty space between contacts, and maximizing total coverage need to be balanced, and an optimal compromise between these design factors may yield an array that most precisely and completely captures interictal activity.

We were also limited to short duration intraoperative recordings. Previous work has validated that HFOs can be captured during intraoperative recordings, and there is evidence that interictal activity, including HFOs, may help fine-tune surgical decisions intraoperatively. 21,23,51 We recorded HFO activity intraoperatively in both awake patients (S3 and S7) and anesthetized patients (S1, S2, S4–S6). Various anesthesia regimens may affect intraoperative ECoG recordings, and studies have specifically shown that propofol may decrease the rate of HFOs, whereas sevoflurane may increase the rate of HFOs. 52-54 We do not see a compelling difference between HFO rate, background activity in the 80-600-Hz band, or HFO amplitude in anesthetized and awake recordings, but more data with control for other variables, such as recording location and type of anesthesia, would be needed to make a strong statistical comparison (Figure S11). It has been shown that HFO activity varies in spatial organization over prolonged intracranial recording times and occurs at the highest rates in non-rapid eye movement sleep stages. 17,55 It should also be noted that although studies of interictal activity from recordings in the epilepsy monitoring unit have indicated that HFOs coincident with interictal discharges, or "spikes," may be especially clinically valuable, we did not find sufficient instances of HFOs coincident with interictal discharges in our recordings to investigate their spatial scale in the present study. 56,57 Interestingly, our previous work also identified intraoperative microseizures in epilepsy patients using the same LCP-TF µECoG arrays.35 Thus, future work using implantable µECoG arrays to record for longer

durations during presurgical monitoring under various states of consciousness will be essential to further understand the clinical relevance of microscale HFOs and their relationship over time to other interictal activity such as interictal discharges and microseizures.

# 5 | CONCLUSIONS

We have shown that cortical arrays that sample epileptic brain both at high resolution and over large areas provide important details of HFO activity that are likely missed by clinical standard macrocontact recordings. Our results provide compelling evidence that HFOs are a phenomenon most often occurring within a 1-mm radius. As the targeting of surgical treatments becomes more spatially precise with the development and adoption of microstimulation and laser ablation, microscale epileptic signals may become even more valuable. Our findings have demonstrated that large coverage  $\mu ECoG$  arrays can precisely capture interictal HFOs and in turn potentially improve the targeting of surgical treatments for drug-resistant epilepsy.

# **AUTHOR CONTRIBUTIONS**

Katrina J. Barth: Conceptualization; data curation; formal analysis; methodology; software; visualization; writing. James Sun: Conceptualization; data curation; methodology; editing. Chia-Han Chiang: Conceptualization; data curation; investigation; methodology; editing. Shaoyu Qiao: Conceptualization; investigation; editing. Charles Wang: Methodology; resources. Shervin Rahimpour: Investigation; methodology; resources; supervision; editing. Michael Trumpis: Conceptualization; methodology; software. Suseendrakumar Duraivel: Data curation; investigation; software; editing. Agrita Dubey: Investigation. Katie E. Wingel: Investigation. Alex E. Voinas: investigation. Breonna Ferrentino: Investigation. Werner Doyle: Funding acquisition; investigation; resources; supervision. Derek G. Southwell: Investigation; resources; editing. Michael M. Haglund: Investigation; resources. Matthew Vestal: Investigation; resources. **Stephen C. Harward:** Investigation; resources. Florian Solzbacher: Funding acquisition; supervision. Sasha Devore: Funding acquisition; investigation; project administration; supervision. Orrin Devinsky: Resources; funding acquisition. Daniel Friedman: Conceptualization; data curation; funding acquisition; project administration; supervision; editing. Bijan Pesaran: Conceptualization; funding acquisition; investigation; methodology; project administration; resources; supervision. Saurabh R. Sinha: Data curation;



funding acquisition; resources; supervision; editing. **Gregory B. Cogan:** Conceptualization; data curation; funding acquisition; investigation; methodology; project administration; supervision; editing. **Justin Blanco:** Conceptualization; methodology; software; supervision; editing. **Jonathan Viventi:** Conceptualization; funding acquisition; investigation; methodology; project administration; supervision; editing.

# **ACKNOWLEDGMENTS**

We would like to thank the patients who participated in this study, as well as Lora Fanda and Beenish Mahmood, who assisted with data collection at NYU Grossman School of Medicine, and Anna Thirakul and Seth Foster, who assisted with data collection at Duke University School of Medicine. K.J.B. received support from the National Science Foundation (Graduate Research Fellowship Program DGE-1644868). J.S. received support from the National Institutes of Health (T32 GM136573), the Vilcek Fellowship, and the American Epilepsy Society. D.F. received support from the National Institutes of Health (R01 NS06209207, R01 NS109367), the Centers for Disease Control and Prevention (U48DP006396-01SIP 19-003), and Epitel. O.D. received support from the National Institutes of Health (R01 MH107396, U01 NS099705, R01 MH111417, U01 NS090415, R01 MH116978, R01 HL151490), Tuberous Sclerosis Alliance, Epilepsy Foundation of America, National Science Foundation, and Finding a Cure for Epilepsy and Seizures (FACES). W.D. received support from the National Institutes of Health (R01 NS062092, R01 MH116978). S.De. received support from the National Institutes of Health (RF1 MH116978, R01 MH111417, R01 NS062092), the Office of Naval Research, and the Templeton World Charity Foundation. B.P. received support from the National Institutes of Health (U01 NS099697, U01 NS099577, U01 NS103518, U01 NS122123, R01 NS104923), the Army Research Office (68984-CS-MUR), and the National Science Foundation (IOS-1557886, IIS-2113271). J.V. received support from the Department of Defense (EP200077), the National Institutes of Health (U01 NS099697, UG3 NS120172, U01 NS123668, R01 DC019498, Clinical and Translational Science Awards grant UL1TR002553), and the National Science Foundation (CBET-1752274). D.G.S. received support from the National Institutes of Health (K12 NS080223) and the Esther A. & Joseph Klingenstein Fund. G.B.C. received support from the Department of Defense (EP200077) and the National Institutes of Health (1UG3NS120172, 1R01-DC019498-01A1, and Clinical and Translational Science Awards grant UL1TR002553). We would also like to thank FACES for providing financial support.

# CONFLICT OF INTEREST STATEMENT

Parts of the technology described here are patent pending under "Electroencephalography (EEG) Electrode Arrays and Related Methods of Use" US Patent Application # PCT/US2020/051400. F.S. declares financial interest in Blackrock Neurotech and Sentiomed, managed by University of Utah's conflict of interest (COI) management. W.D. and D.F. declare financial interest in Neuroview Technology, overseen by NYU Grossman School of Medicine's COI management. D.F. also receives salary support for consulting and clinical trial-related activities performed on behalf of the Epilepsy Study Consortium, a nonprofit organization. D.F. receives no personal income for these activities. NYU receives a fixed amount from the Epilepsy Study Consortium toward D.F.'s salary. Within the past 2 years, the Epilepsy Study Consortium has received payments for research services performed by D.F. from Alterity, Baergic, Biogen, BioXcell, Cerevel, Cerebral, Jannsen, Lundbeck, Neurocrine, SK Life Science, and Xenon. D.F. has also served as a paid consultant for Neurelis Pharmaceuticals and Receptor Life Sciences. O.D. has equity and/or compensation from Privateer Holdings, Tilray, Receptor Life Sciences, Qstate Biosciences, Tevard, Empatica, Engage, Egg Rock/Papa & Barkley, Rettco, SilverSpike, and California Cannabis Enterprises. He has received consulting fees from GW Pharma, Cavion, and Zogenix. S.R.S. has received salary/research support for clinical trials from Eisai, Monteris, Neuropace, UCB, and Sunovion. Within the past 2 years, S.R.S. has received payments for consulting/advisory boards from Acquestive, Basilea, Blackthorn Therapeutics, LivaNova, Monteris, Neuropace, SK Lifesciences, and UCB. The remaining authors have no conflicts of interest to disclose.

## ORCID

Katrina J. Barth https://orcid.org/0000-0002-0193-5057 Chia-Han Chiang https://orcid.

org/0000-0002-4010-1266

Shaoyu Qiao https://orcid.org/0000-0001-7594-6704 Suseendrakumar Duraivel https://orcid.

org/0000-0002-1110-1021

Alex E. Voinas https://orcid.org/0000-0002-4332-2785

Orrin Devinsky https://orcid.org/0000-0003-0044-4632

Saurabh R. Sinha https://orcid.

org/0000-0003-0305-6731

Justin Blanco https://orcid.org/0000-0003-1101-2608 Jonathan Viventi https://orcid. org/0000-0001-6054-0541

# REFERENCES

1. Franco V, French JA, Perucca E. Challenges in the clinical development of new antiepileptic drugs. Pharmacol Res. 2016;103:95–104.



Epilepsia<sup>™</sup> 1923

- 2. Chen Z, Brodie MJ, Liew D, Kwan P. Treatment outcomes in patients with newly diagnosed epilepsy treated with established and new antiepileptic drugs. JAMA Neurol. 2018;75(3):279–86.
- 3. Englot DJ, Birk H, Chang EF. Seizure outcomes in nonresective epilepsy surgery: an update. Neurosurg Rev. 2017;40(2):181–94.
- 4. Franzini A, Moosa S, Servello D, Small I, Dimeco F, Xu Z, et al. Ablative brain surgery: an overview. Int J Hyperthermia. 2019;36(2):64–80.
- 5. Rosenow F. Presurgical evaluation of epilepsy. Brain. 2001;124(9):1683–700.
- Englot DJ, Chang EF. Rates and predictors of seizure freedom in resective epilepsy surgery: an update. Neurosurg Rev. 2014;37:389–404.
- Nair DR, Laxer KD, Weber PB, Murro AM, Park YD, Barkley GL, et al. Nine-year prospective efficacy and safety of brainresponsive neurostimulation for focal epilepsy. Neurology. 2020;95(9):e1244–56.
- 8. Ali R, Air EL. Surgical therapies for epilepsy. In: Spanaki MV, Wasade VS, editors. Understanding epilepsy: a study guide for the boards. Cambridge: Cambridge University Press; 2019. p. 417–31.
- 9. Landazuri P, Shih J, Leuthardt E, Ben-Haim S, Neimat J, Tovar-Spinoza Z, et al. A prospective multicenter study of laser ablation for drug resistant epilepsy one year outcomes. Epilepsy Res. 2020;167:106473.
- Jehi L. The epileptogenic zone: concept and definition. Epilepsy Curr. 2018;18(1):12–6.
- NeuroPace. RNS system physician manual. Mountain View, CA: NeuroPace, Inc; 2020.
- Staba RJ, Stead M, Worrell GA. Electrophysiological biomarkers of epilepsy. Neurotherapeutics. 2014;11:334–46.
- 13. Jacobs J, Levan P, Chander R, Hall J, Dubeau F, Gotman J. Interictal high-frequency oscillations (80-500 Hz) are an indicator of seizure onset areas independent of spikes in the human epileptic brain. Epilepsia. 2008;49(11):1893–907.
- 14. Liu S, Gurses C, Sha Z, Quach MM, Sencer A, Bebek N, et al. Stereotyped high-frequency oscillations discriminate seizure onset zones and critical functional cortex in focal epilepsy. Brain. 2018;141(3):713–30.
- 15. Worrell G, Gotman J. High-frequency oscillations and other electrophysiological biomarkers of epilepsy: clinical studies. Biomark Med. 2011;5(5):557–66.
- Blanco JA, Stead M, Krieger A, Stacey W, Maus D, Marsh E, et al. Data mining neocortical high-frequency oscillations in epilepsy and controls. Brain. 2011;134(10):2948–59.
- 17. Frauscher B, Bartolomei F, Kobayashi K, Cimbalnik J, van 't Klooster MA, Rampp S, et al. High-frequency oscillations: the state of clinical research. Epilepsia. 2017;58(8):1316–29.
- 18. Charupanit K, Sen-Gupta I, Lin JJ, Lopour BA. Amplitude of high frequency oscillations as a biomarker of the seizure onset zone. Clin Neurophysiol. 2020;131(11):2542–50.
- Nevalainen P, von Ellenrieder N, Klimes P, Dubeau F, Frauscher B, Gotman J. Association of fast ripples on intracranial EEG and outcomes after epilepsy surgery. Neurology. 2020;95(16):e2 235–45.
- Jacobs J, Zijlmans M, Zelmann R, Chatillon C-É, Hall J, Olivier A, et al. High-frequency electroencephalographic oscillations correlate with outcome of epilepsy surgery. Ann Neurol. 2010;67(2):209–20.

- 21. van 't Klooster MA, van Klink NEC, Leijten FSS, Zelmann R, Gebbink TA, Gosselaar PH, et al. Residual fast ripples in the intraoperative corticogram predict epilepsy surgery outcome. Neurology. 2015;85(2):120–8.
- 22. Fedele T, van 't Klooster M, Burnos S, Zweiphenning W, van Klink N, Leijten F, et al. Automatic detection of high frequency oscillations during epilepsy surgery predicts seizure outcome. Clin Neurophysiol. 2016;127(9):3066–74.
- 23. van 't Klooster MA, van Klink NEC, Zweiphenning WJEM, Leijten FSS, Zelmann R, Ferrier CH, et al. Tailoring epilepsy surgery with fast ripples in the intraoperative electrocorticogram. Ann Neurol. 2017;81(5):664–76.
- 24. Jacobs J, Wu JY, Perucca P, Zelmann R, Mader M, Dubeau F, et al. Removing high-frequency oscillations. Neurology. 2018;91:1040–52.
- 25. Zweiphenning W, Klooster MAVT, Van Klink NEC, Leijten FSS, Ferrier CH, Gebbink T, et al. Intraoperative electrocorticography using high-frequency oscillations or spikes to tailor epilepsy surgery in The Netherlands (the HFO trial): a randomised, single-blind, adaptive non-inferiority trial. Lancet Neurol. 2022;21(11):982–93.
- Jirsch JD, Urrestarazu E, LeVan P, Olivier A, Dubeau F, Gotman J. High-frequency oscillations during human focal seizures. Brain. 2006;129(Pt 6):1593–608.
- AdTech Product Catalog. In: Corporation A-TMI, editor. MKTG-3006, Rev. Z ed2020.
- Davis TS, Caston RM, Philip B, Charlebois CM, Anderson DN, Weaver KE, et al. Corrigendum: LeGUI: a fast and accurate graphical user Interface for automated detection and anatomical localization of intracranial electrodes. Front Neurosci. 2022;16:858978.
- 29. Sindhu KR, Ngo D, Ombao H, Olaya JE, Shrey DW, Lopour BA. A novel method for dynamically altering the surface area of intracranial EEG electrodes. J Neural Eng. 2023;20(2):026002.
- 30. Bragin A, Engel J Jr, Wilson CL, Fried I, Buzsáki G. High-frequency oscillations in human brain. Hippocampus. 1999;9(2):137–42.
- 31. Schevon CA, Trevelyan AJ, Schroeder CE, Goodman RR, McKhann G, Emerson RG. Spatial characterization of interictal high frequency oscillations in epileptic neocortex. Brain. 2009;132(11):3047–59.
- 32. Worrell GA, Gardner AB, Stead SM, Hu S, Goerss S, Cascino GJ, et al. High-frequency oscillations in human temporal lobe: simultaneous microwire and clinical macroelectrode recordings. Brain. 2008;131(4):928–37.
- Yang JC, Paulk AC, Salami P, Lee SH, Ganji M, Soper DJ, et al. Microscale dynamics of electrophysiological markers of epilepsy. Clin Neurophysiol. 2021;132(11):2916–31.
- 34. Chiang CH, Wang C, Barth K, Rahimpour S, Trumpis M, Duraivel S, et al. Flexible, high-resolution thin-film electrodes for human and animal neural research. J Neural Eng. 2021;18(4):045009.
- 35. Sun J, Barth K, Qiao S, Chiang C-H, Wang C, Rahimpour S, et al. Intraoperative microseizure detection using a high-density micro-electrocorticography electrode array. Brain Commun. 2022;4(3):fcac122.
- Staba RJ, Wilson CL, Bragin A, Fried I, Engel J. Quantitative analysis of high-frequency oscillations (80–500 Hz) recorded in human epileptic hippocampus and entorhinal cortex. J Neurophysiol. 2002;88:1743–52.



- 37. Navarrete M, Alvarado-Rojas C, Le Van Quyen M, Valderrama M. RIPPLELAB: a comprehensive application for the detection, analysis and classification of high frequency oscillations in electroencephalographic signals. PLoS One. 2016;11(6):e0158276.
- 38. Bénar CG, Chauvière L, Bartolomei F, Wendling F. Pitfalls of high-pass filtering for detecting epileptic oscillations: a technical note on "false" ripples. Clin Neurophysiol. 2010;121(3):301–10.
- 39. Amiri M, Lina J-M, Pizzo F, Gotman J. High frequency oscillations and spikes: separating real HFOs from false oscillations. Clin Neurophysiol. 2016;127(1):187–96.
- Witham NS, Reiche CF, Odell T, Barth K, Chiang C-H, Wang C, et al. Flexural bending to approximate cortical forces exerted by electrocorticography (ECoG) arrays. J Neural Eng. 2022;19(4):046041.
- 41. Orsborn AL, Wang C, Chiang K, Maharbiz MM, Viventi J, Pesaran B. Semi-chronic chamber system for simultaneous subdural electrocorticography, local field potentials, and spike recordings. 2015 7th International IEEE/EMBS Conference on Neural Engineering (NER): IEEE; 2015. p. 398–401.
- Blanco JA, Stead M, Krieger A, Viventi J, Marsh WR, Lee KH, et al. Unsupervised classification of high-frequency oscillations in human neocortical epilepsy and control patients. J Neurophysiol. 2010;104:2900–12.
- 43. Worrell GA, Jerbi K, Kobayashi K, Lina JM, Zelmann R, Le Van Quyen M. Recording and analysis techniques for high-frequency oscillations. Prog Neurobiol. 2012;98(3):265–78.
- Gardner AB, Worrell GA, Marsh E, Dlugos D, Litt B. Human and automated detection of high-frequency oscillations in clinical intracranial EEG recordings. Clin Neurophysiol. 2007:118(5):1134–43.
- 45. Roehri N, Lina J-M, Mosher JC, Bartolomei F, Benar C-G. Time-frequency strategies for increasing high-frequency oscillation detectability in intracerebral EEG. IEEE Trans Biomed Eng. 2016;63(12):2595–606.
- 46. Pesaran B, Vinck M, Einevoll GT, Sirota A, Fries P, Siegel M, et al. Investigating large-scale brain dynamics using field potential recordings: analysis and interpretation. Nat Neurosci. 2018;21(7):903–19.
- 47. Buzsáki G, Anastassiou CA, Koch C. The origin of extracellular fields and currents—EEG, ECoG, LFP and spikes. Nat Rev Neurosci. 2012;13:407–20.
- 48. Nelson MJ, Pouget P. Physical model of coherent potentials measured with different electrode recording site sizes. J Neurophysiol. 2012;107(5):1291–300.
- Conrad EC, Tomlinson SB, Wong JN, Oechsel KF, Shinohara RT, Litt B, et al. Spatial distribution of interictal spikes fluctuates over time and localizes seizure onset. Brain. 2019;143:554–69.
- González Otárula KA, von Ellenrieder N, Cuello-Oderiz C,
   Dubeau F, Gotman J. High-frequency oscillation networks

- and surgical outcome in adult focal epilepsy. Ann Neurol. 2019:85(4):485–94.
- 51. Roessler K, Heynold E, Buchfelder M, Stefan H, Hamer HM. Current value of intraoperative electrocorticography (io-pECoG). Epilepsy Behav. 2019;91:20–4.
- Chui J, Manninen P, Valiante T, Venkatraghavan L. The anesthetic considerations of intraoperative electrocorticography during epilepsy surgery. Anesth Analg. 2013;117(2):479–86.
- Zijlmans M, Huiskamp GM, Cremer OL, Ferrier CH, Van Huffelen AC, Leijten FSS. Epileptic high-frequency oscillations in intraoperative electrocorticography: the effect of propofol. Epilepsia. 2012;53(10):1799–809.
- 54. Orihara A, Hara K, Hara S, Shimizu K, Inaji M, Hashimoto S, et al. Effects of sevoflurane anesthesia on intraoperative high-frequency oscillations in patients with temporal lobe epilepsy. Seizure. 2020;82:44–9.
- Gliske SV, Irwin ZT, Chestek C, Hegeman GL, Brinkmann B, Sagher O, et al. Variability in the location of high frequency oscillations during prolonged intracranial EEG recordings. Nat Commun. 2018;9(1):2155.
- Guth TA, Kunz L, Brandt A, Dümpelmann M, Klotz KA, Reinacher PC, et al. Interictal spikes with and without highfrequency oscillation have different single-neuron correlates. Brain. 2021;144:3078–88.
- 57. Wang S, So NK, Jin B, Wang IZ, Bulacio JC, Enatsu R, et al. Interictal ripples nested in epileptiform discharge help to identify the epileptogenic zone in neocortical epilepsy. Clin Neurophysiol. 2017;128(6):945–51.

# SUPPORTING INFORMATION

Additional supporting information can be found online in the Supporting Information section at the end of this article.

How to cite this article: Barth KJ, Sun J, Chiang C-H, Qiao S, Wang C, Rahimpour S, et al. Flexible, high-resolution cortical arrays with large coverage capture microscale high-frequency oscillations in patients with epilepsy. Epilepsia. 2023;64:1910–1924. https://doi.org/10.1111/epi.17642

